NeuroToxicology 34 (2013) 243–253

Contents lists available at SciVerse ScienceDirect

NeuroToxicology

Neurotoxic potential of iron oxide nanoparticles in the rat brain striatum and hippocampus

Jie Wu [1], Tingting Ding [1], Jiao Sun [*]

Shanghai Biomaterials Research and Testing Center, Shanghai Key Laboratory of Stomatology, Ninth People's Hospital, Shanghai Jiaotong University School of Medicine, Shanghai 200023, China

ARTICLE INFO

Article history:
Received 27 April 2012
Accepted 10 September 2012
Available online 18 September 2012

Keywords:
Iron oxide nanoparticles
Striatum
Hippocampus
Oxidative stress
Dopaminergic neuron
Neurotoxicity
JNK
p53

ABSTRACT

It has recently been reported that iron oxide nanoparticles (Fe_3O_4-NPs, 30 nm) have the ability to translocate directly from the olfactory nerve to the brain. The striatum and hippocampus are important structures in the brain and are associated with the development of Parkinson's and Alzheimer's diseases. Therefore, it is critical to evaluate Fe_3O_4-NPs and their potential to confer striatum and hippocampus neurotoxicity. This study focuses on the effects of Fe_3O_4-NPs on the striatum and hippocampus, including oxidative injury and the accumulation and retention of Fe_3O_4-NPs. This study also explores the molecular mechanism of oxidative damage in dopaminergic neurons; we were able to assess the neurotoxic effects of Fe_3O_4-NPs by incubating dopaminergic neurons with radioactive Fe_3O_4-NPs. A regional distribution of Fe_3O_4-NPs was observed in rat brains after the particles were intranasally instilled for seven days. The particles were found to be deposited at particularly high concentrations in the rat striata and hippocampi. Over half of the Fe_3O_4-NPs were retained in the striata for a minimum of 14 days, and may have induced oxidative damage to the region. However, no injuries were observed in the hippocampi. These *in vitro* studies demonstrate that Fe_3O_4-NPs may decrease neuron viability, trigger oxidative stress, and activate JNK- and p53-mediated pathways to regulate the cell cycle and apoptosis. These results also suggest that environmental exposure to Fe_3O_4-NPs may play a role in the development of neurodegenerative diseases.

1. Introduction

In the past several years, there have been numerous toxicological investigations of aerodynamic nanoparticles and their impact on occupational health and the environment (Liao et al., 2009; Maynard and Kuempel, 2005). It has recently been reported that inhaled nanoparticles either translocate directly into the brain or exit the lungs and enter the circulation (Oszlánczi et al., 2011). Silver (Takenaka et al., 2001), ultrafine carbon black (ufCB) (Tin Tin Win et al., 2006), manganese (Mn) oxide (Elder et al., 2006), and titanium dioxide (TiO_2) nanoparticles (Wang et al., 2008a,b) have been found to translocate into the brain via the olfactory nerve. These nanoparticles are reported to cause inflammation and impair neural function in the hippocampus (Tin Tin Win et al., 2006; Elder et al., 2006; Wang et al., 2008a,b,c). As a result, it is imperative to assess the potential of these nanoparticles to contribute to neurotoxicity.

Iron oxide nanoparticles (Fe_3O_4-NPs) have recently attracted extensive interest due to their superparamagnetic physicochemical properties and potential applications in the biomedical and industrial fields. These applications include biomedical brain imaging, brain-targeted drug or gene delivery, catalysis, and magnetic storage (Hood, 2004). Previous studies have proposed that Fe_3O_4-NPs could be transported via the olfactory nerve tract to the brain, causing oxidative stress and ultrastructural alterations in the olfactory bulb nerve cells (Wang et al., 2009). Little is known about the accumulation, retention, and adverse effects of Fe_3O_4-NPs on the brain; the nanoparticles' effects on the striatum and hippocampus, which are involved in neurodegenerative conditions such as Parkinson's and Alzheimer's diseases, are also unknown. The striatum regulates movement pathways and is involved in various cognitive processes. The hippocampus contributes to long-term memory and spatial navigation. Although Fe_3O_4-NP-induced cytotoxicity has been studied in PC12 cells (Pisanic et al., 2007), the precise neural damage pathways and cytotoxicity mechanisms are still ill-defined.

In the present study, we tested the hypothesis that Fe_3O_4-NP exposure induces *in vivo* and *in vitro* neurotoxicity. The distribution, accumulation and retention of intranasally instilled Fe_3O_4-NPs in the brain were detected via stable isotopic tracing (Xie et al.,

* Corresponding author. Tel.: +86 21 63034903.
E-mail address: jiaosun59@yahoo.com (J. Sun).
[1] These authors contributed equally to this work.

0161-813X/$ – see front matter © 2012 Elsevier Inc. All rights reserved.
http://dx.doi.org/10.1016/j.neuro.2012.09.006

2010). The tracing techniques were performed as described in previously published articles from this laboratory. Fe_3O_4-NPs were incubated with dopaminergic neuronal PC12 cells in *in vitro* studies that were based on the *in vivo* studies. The adverse impact of Fe_3O_4-NPs on cell viability, oxidative stress, apoptosis and cell signalling pathways were investigated in these dopaminergic neurons.

2. Materials and methods

2.1. Characterisation of Fe_3O_4-NPs

Fe_3O_4-NPs at ≥99.0% purity were purchased from the Sigma Chemical Company (Saint Louis, MO, USA). The average size of the nanoparticles was confirmed by transmission electron microscopy (TEM, JEM-2010, JEOL Ltd., Tokyo, Japan). The sizes and charges of the nanoparticles and agglomerates were also measured by dynamic light scattering (DLS) and zeta potential, respectively. Nanoparticles were suspended in physiological saline or high glucose Dulbecco's modified Eagle's medium (DMEM) with 10% fetal bovine serum (FBS); the nanoparticle measurements were taken on a ZetaSizer (Malvern Instruments Ltd., Worcestershire, UK).

2.2. In vivo *studies: radiolabelling of Fe_3O_4-NPs with ^{125}I*

The ^{125}I radiolabelling of the Fe_3O_4-NPs was based on a protocol from a report (Xie et al., 2010). Amino groups were added to the Fe_3O_4-NPs via aminopropyltriethoxysilane (APTS) modification. The modified Fe_3O_4-NPs were then incubated with Bolton–Hunter (BH) reagent, dimethylformamide and $Na^{125}I$ suspended in chloramine. The radiolabelling reaction was terminated by the addition of glycine-supplemented borate buffer. The ^{125}I-Fe_3O_4-NPs were ultimately separated by column chromatography and characterised by TEM and Zetasizer. We used instant thin layer chromatography–silica gel (ITLC-SG) and a γ-counter to identify the ^{125}I-Fe_3O_4-NPs in solution (Shanghai Institute of Nuclear Instrument Factory, China). Prior to the *in vivo* assay, the stability of ^{125}I-Fe_3O_4-NPs was analysed in 37 °C physiological saline containing 10% (v%) rat serum. Two microliter samples of the ^{125}I-Fe_3O_4-NP suspension were extracted at five time points after instillation (1, 3, 7, 15, and 30 days) and analysed by ITLC-SG paper chromatography. The stability of the ^{125}I-Fe_3O_4-NPs was expressed as a percentage of radioactivity at the site of instillation compared with the total radioactivity.

2.3. In vivo *animal studies*

Our animal studies were approved by the Animal Ethical Committee of Shanghai Jiaotong University (China), where they inspected for any clinical signs. Four-week-old male SD rats (Appenzeller et al., 2008; Yamauchi et al., 2000) were purchased from SLACCAS Laboratory Animal Co., Ltd. (Shanghai, China). Six rats per cage were housed in controlled environmental conditions (temperature 23 ± 0.5 °C, humidity 50 ± 5%, lights on 07:00–19:00 h). Rodent diet and water were provided ad libitum. The experiments were initiated one week after the arrival of the animals.

2.4. In vivo *studies: studies of intranasally instilled Fe_3O_4-NPs in rat brains*

As shown in Fig. 1, the rats in our studies were divided into four groups: (1) intranasally instilled with ^{125}I-Fe_3O_4-NPs for 1 day (In1d, euthanised at 1 d); (2) intranasally instilled with ^{125}I-Fe_3O_4-NPs for 7 days (In7d, euthanised at 8 d); (3) 7 days post-instillation (post in 7d, euthanised at 14 d); (4) 14 days post-instillation (post in 14d, euthanised at 21 d). ^{125}I-Fe_3O_4-NPs were suspended in physiological saline (1 mg/ml) and sonicated with a Hilscher UP200S (Hilscher Ultrasonics GmbH, Teltow, Germany); this sonicator generates ultrasonic pulses of 600 W at 20 kHz and was used to sonicate the nanoparticles for 30 min to prevent aggregation prior to nasal instillation. Supine rats were lightly anaesthetised with sodium pentobarbital, and 10 μg (in 10 μl) of ^{125}I-Fe_3O_4-NPs was intranasally instilled in each rat nostril (20 μg total). Six animals were euthanised at each time point (2 d, 8 d, 14 d, and 21 d, Fig. 1) after weighed, and brain tissues were perfused from every animal. Regions of the sub-brain – including the olfactory bulb, striatum, hippocampus, frontal cortex, cerebellum and brain stem – were separated, gathered, weighed, and counted in a γ-counter for 15 min to measure radioactivity.

2.5. In vivo *studies: oxidative stress-related biomarker assay*

The striatum and hippocampus are key regions of the brain that were examined for injuries following nanoparticle instillation. The six-striatum and hippocampus samples in each group were weighed and suspended in cold protein lysis buffer when the samples were at the ratio of 1:9 (w/v). The protein lysis buffer included 50 mM Tris pH 7.4, 150 mM NaCl, 1 mM EDTA, 1 mM EGTA, 5% 2-mercaptoethanol, 1% NP-40, 0.25% sodium deoxycholate, 5 μg/ml leupeptin, 5 μg/ml asprotinin, 10 μg/ml soybean trypsin inhibitor and 0.2 mM phenylmethyl sulfonyl-fluoride. Each tissue mixture was homogenised four times with an ultrasonic cell disruptor (Sonics Vibra-Cell, VCX105) for 8 s intervals at 4 °C. The solution was centrifuged at 14,000 × *g* for 5 min at 4 °C, and the resulting supernatant was collected for oxidative biomarker analysis. Striatum and hippocampus extracts were examined for glutathione reductase (GSH-PX) and superoxidase dismutase (SOD) activity; the levels of hydrogen peroxide (H_2O_2) and malondiadehyde (MDA) were also analysed according to the manufacturer's instructions. All commercial colorimetric assay kits were purchased from Beyotime Biotech (Nantong, China).

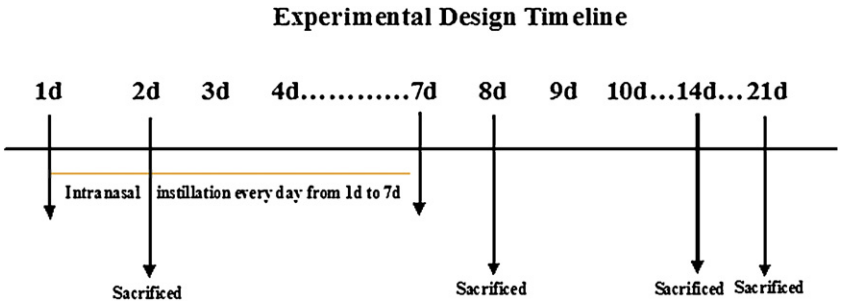

Fig. 1. Experimental design for the intranasal instillation (IN) of Fe_3O_4-NPs in rats.

2.6. In vivo *studies: histopathological examination*

Six animals in each group were euthanised at the time points shown in Fig. 1. All of the rat brains – including the negative control into which 0.9% sodium chloride was injected – were excised and immediately fixed in a 10% formalin solution. Histopathological examinations were conducted using standard laboratory procedures. The brains were embedded in paraffin blocks, sectioned into 5-μm-thick slices, mounted on the microscope glass slides and stained with haematoxylin–eosin (HE). The sections were then observed under optical microscopy and photographed. All of the tissue samples were anonymised during the pathology analysis.

2.7. In vitro *studies: PC12 cell culture treatment with Fe_3O_4-NPs*

PC12 cells were obtained from the Cell Bank of Type Culture Collection of Chinese Academy of Sciences in Shanghai. The cells were grown in high-glucose DMEM (Gibco-Invitrogen Company, Paisley, UK) at 37 °C in 5% CO_2. The growth medium contained 10% FBS, 100 U/ml penicillin, 100 μg/ml streptomycin (Gibco-Invitrogen Company, Paisley, UK) and 50 ng/ml nerve growth factor (NGF-2.5S, Sigma Chemical Company, Saint Louis, MO, USA).

Fe_3O_4-NPs were sterilised by incubation at 120 °C for 2 h and suspended in culture medium. This stock solution was then serially diluted into doses ranging from 25 to 200 μg/ml. These samples were sonicated for a minimum of 30 min to produce a uniform suspension. Freshly sonicated Fe_3O_4-NP suspensions were immediately applied to cells that had attached for 24 h in complete medium. The cells in the control *in vitro* assay group were not mixed with Fe_3O_4-NPs.

2.8. In vitro *studies: MTT assay and LDH measurements*

The mitochondrial function and cell viability of PC12 cells cultured in media containing different concentrations of Fe_3O_4-NPs (25, 50, 100 and 200 μg/ml) were measured by the MTT [3-(4,5-dimethylthiazol-2-yl)-2,5-diphenyltetrazolium bromide, Sigma Chemical Company, Saint Louis, MO, USA] assay. In the MTT assay, cells were plated into a 96-well plate at a density of 2×10^4 cells/well; the cells were suspended in 200 μl of culture medium and allowed to attach for 24 h before treatment. The cell culture medium was then replaced with 200 μl of nanoparticle suspensions; the cells were subsequently incubated for 24 h. Next, 20 μl of MTT (0.5 mg/ml) was added to each well, and the cells were incubated at 37 °C for another 4 h. Mitochondrial dehydrogenases from the viable cells reduced water-soluble MTT to water-insoluble formazan crystals, which were then solubilised with dimethyl sulfoxide (DMSO, Sigma Chemical Company, Saint Louis, MO, USA). The cell culture medium was aspirated carefully, after which 150 μl DMSO was added and mixed thoroughly in each well. The optical density (OD) was read on an ELISA reader (Wellscans MK3, Thermo Labsystems, Finland) at 570 nm using 630 nm as the reference. The final results are expressed as a viability percentage of readings from the untreated controls.

Lactate dehydrogenase (LDH) leakage is based on levels of LDH activity in the extracellular medium; this parameter serves as another marker of cell viability. After being mixed with different concentrations of Fe_3O_4-NPs for 24 h, the culture medium was collected and centrifuged at 3000 rpm for 5 min to obtain a cell-free supernatant. The activity of LDH in the medium was determined using a commercial LDH Kit (Jiancheng, Nanjing, China) according to the manufacturer's protocol; the optical absorption of the medium was then measured at

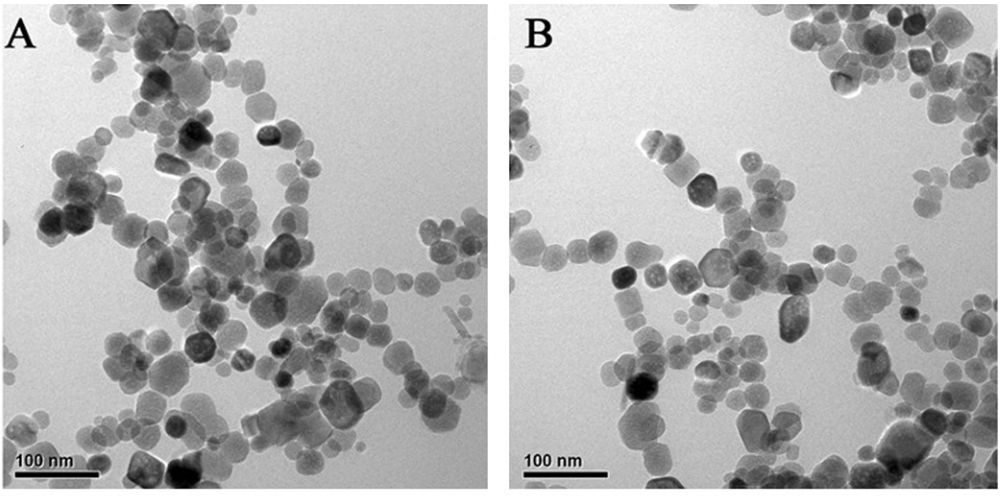

C

Particles	Mean size (nm)		Zeta potential (mv)
	TEM	DLS	
Fe_3O_4-NPs	30	physiological saline : 496 ±86	-9.1 ±2.2
		DMEM with 10% FBS: 570 ±103	-8.5 ±1.7
Fe_3O_4-NPs-^{125}I	36	physiological saline : 462 ±75	-8.4 ±2.1

Fig. 2. Characterisation data of Fe_3O_4-NPs and ^{125}I-Fe_3O_4-NPs. (A) Transmission electron microscopy (TEM) analysis of Fe_3O_4-NPs; (B) TEM analysis of ^{125}I-Fe_3O_4-NPs; (C) particle size, hydrodynamic diameter and zeta potential of Fe_3O_4-NPs and ^{125}I-Fe_3O_4-NPs.

440 nm using a UV–vis spectrophotometer (TianMei UV-8500, Shanghai, China).

2.9. In vitro *studies: intracellular ROS measurement and oxidative damage*

The production of intracellular reactive oxygen species (ROS) was measured using the fluorescent probe 2′,7′-dichlorofluorescein diacetate (DCFH-DA). DCFH-DA passively enters cells and reacts with ROS to form the highly fluorescent compound dichlorofluorescein (DCF). A DCFH-DA stock solution (10 mM in methanol, Beyotime Biotech, Nantong, China) was diluted 1000-fold in serum-free DMEM to yield a 10 μM working solution. PC12 cells were seeded at a density of 5.0×10^5 cells/well in 6-well plates. After 6 h of exposure to Fe_3O_4-NPs at 25, 50, 100 and 200 μg/ml, the cells were incubated in 2 ml of DCFH-DA working solution at 37 °C for 30 min. The fluorescence levels were then determined with a flow cytometer (Becton Dickinson, San Jose, CA, USA).

The levels of GSH-PX, SOD and MDA were measured using reagent kits (Beyotime Biotech, Nantong, China). PC12 cells were plated into 6-well plates at a density of 5.0×10^5 cells/well and treated with Fe_3O_4-NPs; the nanoparticle suspensions were applied at concentrations of 25, 50, 100 and 200 μg/ml. After the cells were treated with Fe_3O_4-NPs for 24 h, the intracellular levels of GSH-PX, SOD and MDA were measured with reagent kits according to the manufacturer's instructions. Specifically, PC12 cells were mixed with 40 μl of metaphosphoric acid and centrifuged at 10,000 × *g* for 10 min at 4 °C. The resulting supernatant was used for the GSH-PX assay. The GSH-PX levels were measured using the DTNB-GSSG recycling assay. The SOD activity was measured at 550 nm after samples were treated with 2% SDS.

2.10. In vitro *studies: measurements of apoptosis*

Apoptosis in PC12 cells was analysed using an annexin V-FITC/propidium iodide (PI) apoptosis detection kit (BD PharMingen, San Jose, CA, USA). The PC12 cells were first placed into 6-well plates at a density of 5.0×10^5 cells/well. After being exposed to various concentrations of Fe_3O_4-NPs for a total of 24 h, the cells were then washed three times with PBS. The PC12 cells were removed with trypsin and centrifuged at 1000 rpm. The cell pellets were resuspended in 1× binding buffer and stained with annexin V-FITC; the staining protocol was performed as recommended by the manufacturer. Subsequently, these samples were diluted with 1× binding buffer and analysed with a FACScan flow cytometer (Becton Dickinson, San Jose, CA).

2.11. In vitro *studies: measurements of cell cycle*

For the cell cycle analysis, PC12 cells were plated into a 6-well plate at a density of 5.0×10^5 cells/well. After 24 h of exposure to the Fe_3O_4-NPs, the cells were collected, fixed, permeabilised with 75% ice cold ethanol, and stored at 20 °C. The cells were then resuspended in 1 ml of lysis buffer (0.1% Triton X-100, 0.05 mg/ml propidium iodide, and 1 mg/ml RNase A), incubated for 30 min at 37 °C, and analysed with a flow cytometer for DNA content.

2.12. In vitro *studies: Western blot analysis*

PC12 cells were stimulated for 24 h with 25, 50, 100 or 200 μg/ml of Fe_3O_4-NPs. After nanoparticle incubation, the cells were lysed in ice-cold protein lysis buffer (50 mM Tris pH 7.4, 150 mM NaCl, 1 mM EDTA, 1 mM EGTA, 5% 2-mercaptoethanol, 1% NP-40, 0.1% sodium dodecyl sulfate (SDS), 5 μg/ml leupeptin, 5 μg/ml aprotinin, 10 μg/ml soybean trypsin inhibitor and 0.2 mM phenylmethyl sulfonylfluoride) for 30 min. The protein lysis buffer was mixed with phosphatase inhibitor cocktail (Sigma, Saint Louis, MO, USA) to evaluate protein phosphorylation. After centrifuging the lysates for 10 min at 12,000 rpm at 4 °C, the supernatants were collected and stored at 80 °C. Protein concentrations were determined with the BCA assay (Pierce, Rockford, USA). About

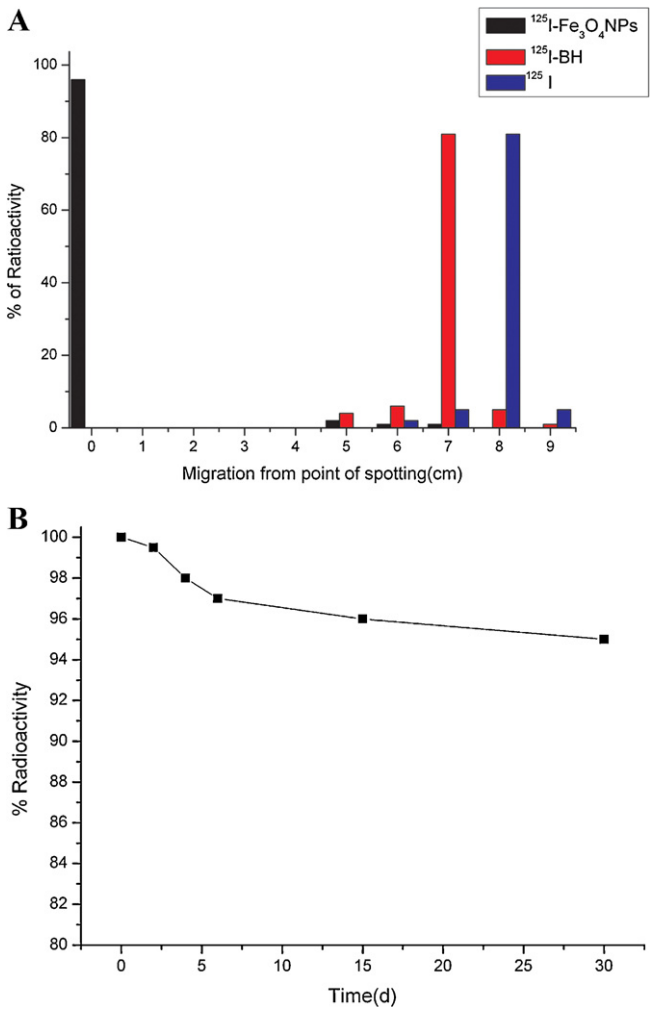

Fig. 3. Identification and stability of ^{125}I-Fe_3O_4-NPs. (A) Identification of ^{125}I-Fe_3O_4-NPs by ITLC-SG; (B) stability of ^{125}I-Fe_3O_4-NPs suspended for 30 days in physiological saline solution containing 10% rat serum.

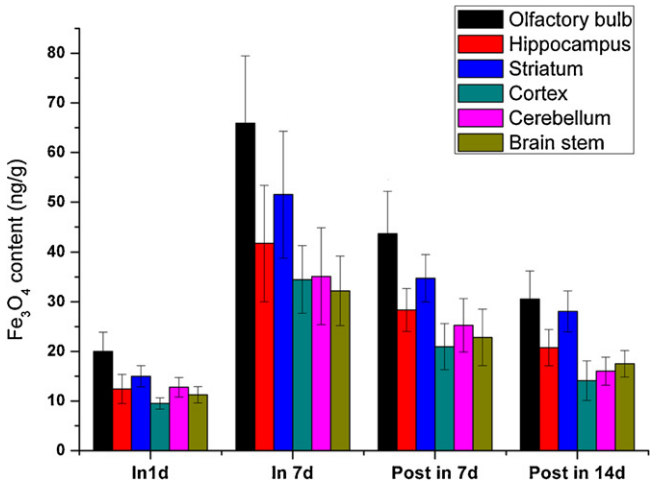

Fig. 4. Fe_3O_4-NP content in rat brains ($n = 6$) after intranasal and post instillation.

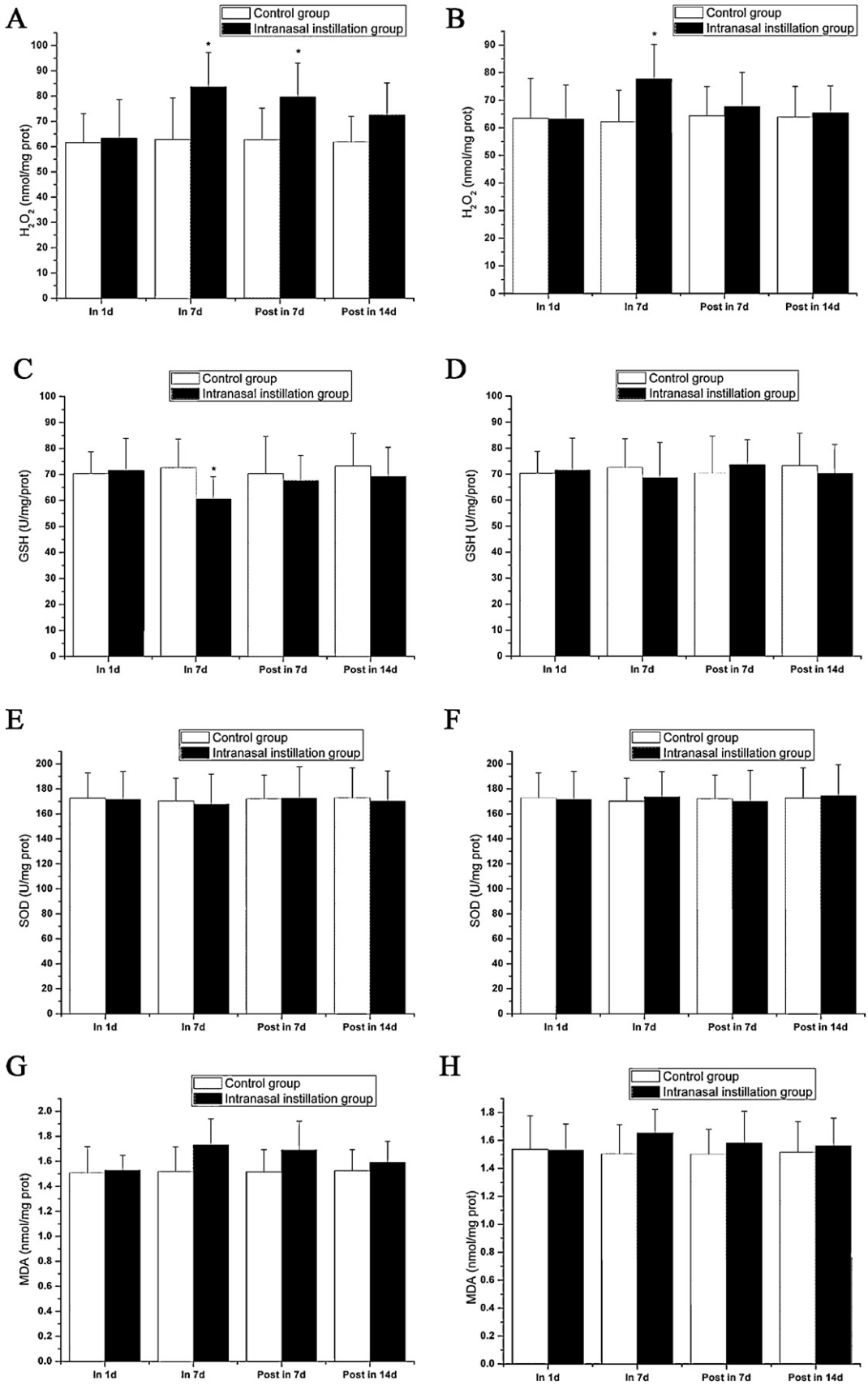

Fig. 5. H_2O_2, GSH-PX, SOD, and MDA levels in striata and hippocampi ($n = 6$) in rats that were intranasally instilled with Fe_3O_4-NPs; figures illustrate nanoparticle levels in brains that were instilled for 1 day and 7 days, post-instillation 7 and 14 days (A, C, E and G: H_2O_2 GSH-PX, SOD, and MDA levels within the striatum; B, D, F and H: H_2O_2 GSH-PX, SOD, and MDA levels within the hippocampus. $^*p < 0.05$ *vs.* control).

30–50 μg protein was separated by sodium dodecyl sulphate–polyacrylamide gel electrophoresis (SDS-PAGE) and electrophoretically transferred to polyvinylidene difluoride (PVDF) membranes (Millipore). The membranes were blocked for 1 h at room temperature in Tris-buffered saline (TBS) containing 0.05% Tween-20 (TBST) and 5% nonfat milk. The membranes were then incubated overnight at 4 °C with anti-phosphorylated-JNK (p-JNK), anti-JNK, anti-phosphorylated-c-Jun (p-c-Jun), anti-c-Jun, bax, bcl-2 (Bioworld Technology Inc., USA), anti-phosphorylated-p53 (p-p53), anti-p53 (Cell Signaling Technology, Beverly, MA, USA), anti-p21, anti-Gadd45 and anti-β-actin (Santa Cruz Biotechnology, Santa Cruz, CA, USA). The membranes were subsequently washed with TBST and incubated with a horseradish peroxidase-conjugated anti-rabbit or anti-mouse IgG (Cell Signaling Technology, Beverly, MA, USA) secondary antibody for 1 h at 37 °C; an enhanced chemiluminescence kit (Millipore, USA) was used to process the membranes. Bio-Rad Quantity One software (Bio-Rad, Richmond, CA) was used to densitometrically detect post-transcriptional modifications such as p-JNK, p-c-Jun, bax and p-p53.

2.13. Data analysis

The sample radioactivity was determined using the equation $C = C_0 \times e^{-(0.693159t/T)}$ (with C being the actual radioactivity, C_0 is the measured radioactivity, T is the half-life of ^{125}I (59.6 days), and t the time interval between C and C_0). The data were expressed as the means ± SD. The statistical analyses were performed using SPSS 12.0, and the statistical comparisons were analysed by the Student's t-test. The differences were considered to be statistically significant when the p-values were less than 0.05.

3. Results

3.1. Characterisation, identification and stability of Fe_3O_4-NPs and ^{125}I-Fe_3O_4-NPs

The Fe_3O_4-NPs employed in this study were measured by TEM to be 30 nm in size (Fig. 2A) and remained spherical after being labelled with ^{125}I (Fig. 2B). The hydrodynamic diameters of the Fe_3O_4-NPs and ^{125}I-Fe_3O_4-NPs in physiological saline were 496 ± 86 nm and 462 ± 75 nm, respectively (Fig. 2C). Zeta potential determination revealed that the Fe_3O_4-NPs and ^{125}I-Fe_3O_4-NPs were −9.1 ± 2.2 mV and −8.4 ± 2.1 mV in physiological saline, respectively (Fig. 2C). Statistical comparisons showed no significant increases in size or zeta potential in the labelled particles ($p > 0.05$).

^{125}I moved toward the solvent front (Rf = 0.9) faster than ^{125}I-BH (Rf = 0.7), but the ^{125}I-Fe_3O_4-NPs remained at the point of spotting (Rf = 0) with the labelling yield reaching 95% (Fig. 3A). Radiolabelling stability is important for accurate results; Fig. 3B shows that the ^{125}I-Fe_3O_4-NPs were stable for 30 d *in vitro* and consistently exceeded 95% in purity.

3.2. Biodistribution, accumulation and retention studies

During the experimental period, no animals exhibited any signs of acute toxicity or clinical signs of abnormalities. In addition, none

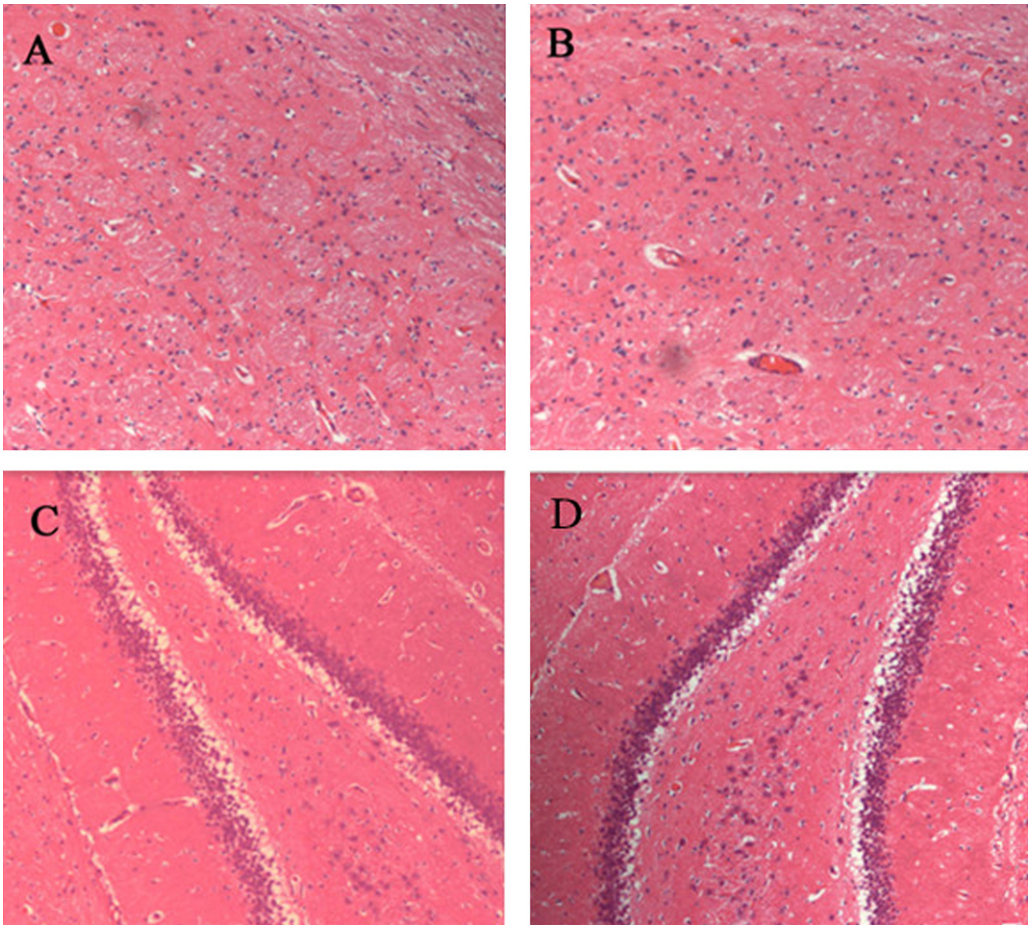

Fig. 6. Histopathology of rat brain tissue after 7 days of repeated intranasal instillation with Fe_3O_4-NPs in physiological saline. (A) The striatum region of the control group; (B) the striatum region of the intranasal instillation group; (C) the hippocampal region of the control group; (D) the hippocampal region of the intranasal instillation group. The sections were stained with H&E and observed under a light microscope at 10x magnification.

of the animals died during the test period. The sub-brain region radioactivity was expressed in units of ng/g of tissue. The sub-brain regions were measured for Fe_3O_4-NP deposition on the seventh day of instillation exposure. Fig. 4 shows that the nanoparticles were deposited from highest to lowest concentration in the olfactory bulb, striatum, hippocampus, brain stem, cerebellum, and frontal cortex, respectively. There were no significant changes in any of the sub-brain regions ($p > 0.05$), except in the olfactory bulb. Fig. 4 shows a significant increase in nanoparticle deposition from 1 d to 7 d of instillation exposure ($p < 0.05$). The clearance of Fe_3O_4-NPs from the brain regions was slow, as more than half of the Fe_3O_4-NPs in the striatum and hippocampus remained 14 days post-instillation.

3.3. Oxidative damage in the brain

Seven days after the nanoparticles were instilled in the striatum, we observed significant changes in oxidative damage markers (H_2O_2, SOD and MDA, $p < 0.05$) compared with controls (Fig. 5). Significant differences between the control and experimental groups in the striatum levels of GSH were detected 7 days following instillation ($p < 0.05$). The levels of H_2O_2 in the hippocampal and stratum tissue following 7 days of instillation were significantly different from those of the control ($p < 0.05$). However, there were no significant changes in the two other markers in the hippocampal tissue at any of the time points (Fig. 5).

3.4. Pathology changes

Histopathological examination showed that no significant exposure-related brain lesions were present in rat brains intranasally instilled with Fe_3O_4-NPs compared with lesions in physiological saline-exposed controls. This finding was observed upon examining rat brains at all experimental time points. The histopathological tests performed on the 7 days instillation and the corresponding control groups are outlined in Fig. 6.

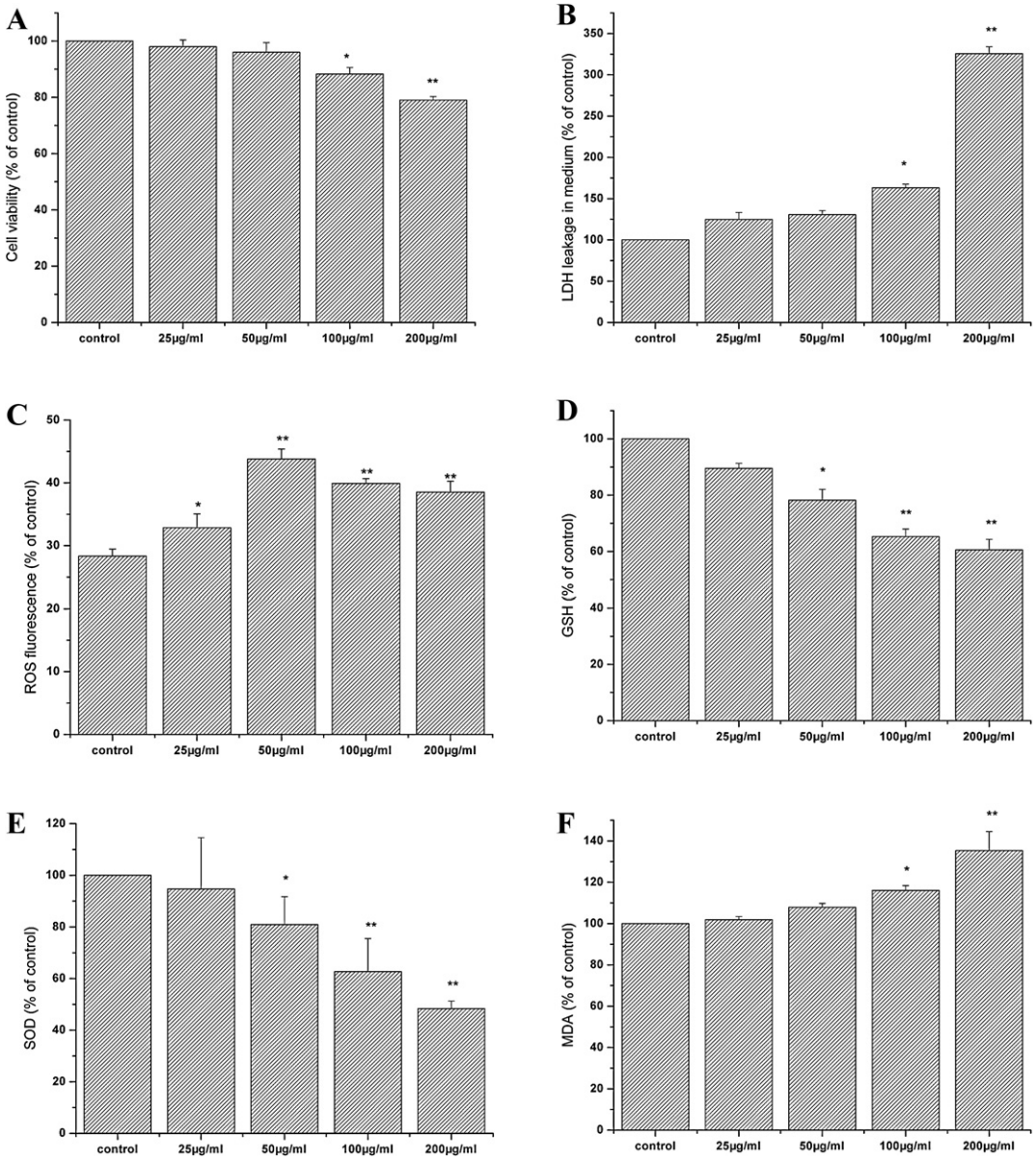

Fig. 7. The effect of Fe_3O_4-NPs on the viability, LDH levels and oxidative stress of PC12 cells. (A) The viability of PC12 cells treated with different concentrations of Fe_3O_4-NPs for 24 h as measured by the MTT assay; (B) the LDH level of PC12 cells cultured in media containing Fe_3O_4-NPs for 24 h; (C) ROS production (incubation time, 6 h) after treatment with Fe_3O_4-NPs; (D, E); and (F) PC12 levels of GSH-PX, SOD and MDA (incubation time, 24 h) after Fe_3O_4-NP treatment ($n = 3$, $^*p < 0.05$ *vs.* control).

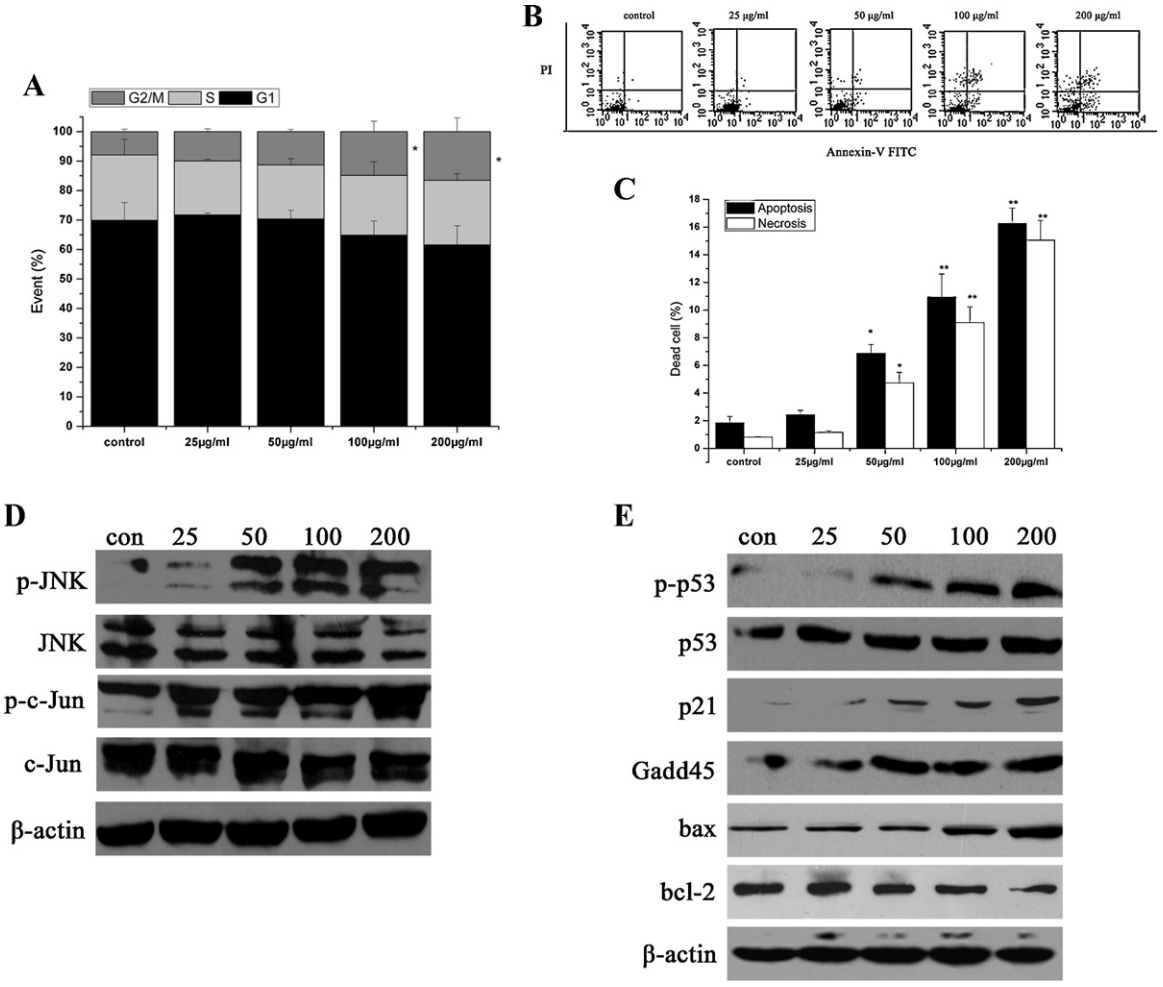

Fig. 8. Analysis of the cell cycle, apoptosis and the molecular mechanism of PC12 cells treated with Fe_3O_4-NPs. (A) The cell cycle distribution of PC12 cells cultured with Fe_3O_4-NPs; (B and C) apoptosis and necrosis of PC12 cells as induced by Fe_3O_4-NP treatment; cells are double stained with PI and FITC-labelled annexin V; (E) Western blot analysis of p53, p-p53, p21, Gadd45, bax and bcl-2 expression in PC12 cells; expression was induced by PC12 exposure to Fe_3O_4-NPs; (D) Western blot analysis of p-JNk, JNK, p-c-Jun, and c-Jun expression in PC12 cells, which were induced by Fe_3O_4-NPs ($n = 3$, $^*p < 0.05$ *vs.* control, $^{**}p < 0.01$ *vs.* control).

3.5. Cytotoxic and oxidative stress of Fe_3O_4-NPs on PC12 cells

As shown in Fig. 7A, the PC12 cell viability decreased after 24 h as a function of Fe_3O_4-NPs dosage levels. Significant cytotoxicity was observed when PC12 cells were incubated with Fe_3O_4-NPs (100 and 200 μg/ml) for 24 h ($p < 0.05$ and $p < 0.01$, respectively). Fe_3O_4-NPs induced Lactate dehydrogenase (LDH) leakage from PC12 cells that were treated for 24 h; this leakage reveals the effect of nanoparticles on cell membrane integrity. After PC12 cells were incubated with nanoparticles at concentrations of 100 and 200 μg/ml, the LDH levels in the cell medium were significantly elevated compared with those in control conditions (Fig. 7B). The ROS results indicate that the DCF fluorescence intensity increased after 6 h of Fe_3O_4-NPs exposure (Fig. 7C). The intracellular levels of GSH-PX and SOD in PC12 cells exhibited a dose-dependent decrease after 24 h of exposure to Fe_3O_4-NPs (Fig. 7D and E). Fe_3O_4-NPs elevated the intracellular MDA concentration in a dose-dependent manner (Fig. 7F).

Table 1
Densitometry analysis for Western blot ($n = 3$).

Protein	Group (μg/ml)				
	Con	25	50	100	200
P-JNk	13.86 ± 1.02	14.94 ± 0.89	21.69 ± 1.96*	24.70 ± 1.29*	24.80 ± 1.45*
JNK	21.30 ± 1.54	19.71 ± 0.82	20.43 ± 1.54	19.88 ± 1.07	18.65 ± 1.35
p-c-Jun	15.85 ± 0.95	18.20 ± 1.69	18.36 ± 1.23	24.22 ± 1.76*	23.34 ± 1.49*
c-Jun	19.43 ± 0.87	19.25 ± 1.47	20.19 ± 1.01	19.84 ± 1.14	21.26 ± 1.93
p-p53	14.84 ± 1.35	16.09 ± 1.94	21.13 ± 2.19*	22.74 ± 1.75*	25.18 ± 1.46*
p53	19.81 ± 2.01	20.44 ± 1.50	19.72 ± 0.96	19.47 ± 1.04	20.53 ± 1.08
p21	15.77 ± 1.24	17.14 ± 1.28	21.12 ± 1.67	22.48 ± 1.24*	23.47 ± 1.99*
Gadd45	13.31 ± 0.94	16.92 ± 0.87	21.18 ± 1.84*	23.02 ± 1.83*	25.54 ± 1.80*
bax	14.62 ± 1.23	17.73 ± 1.10	18.06 ± 1.07	23.11 ± 2.13*	26.44 ± 1.35*
bcl-2	23.21 ± 1.95	20.15 ± 1.54	20.05 ± 1.62	19.53 ± 1.09*	17.04 ± 1.13*

* $p < 0.05$ *vs.* control.

3.6. The mechanism of Fe_3O_4-NPs on cell apoptosis and cell cycle arrest

Cell cycle analysis showed that Fe_3O_4-NPs have an effect on G2/M arrest (Fig. 8A). The apoptosis rate also increases from 1.84% to 16.25% in the control group compared with cells exposed to 200 μg/ml of Fe_3O_4-NPs for 24 h (Fig. 8B and C), respectively. To determine the mechanisms of Fe_3O_4-NP-induced apoptosis and G2/M arrest, we examined the expression of apoptosis and cell cycle regulators in PC12 cells. Our results demonstrate an increase in JNK and c-Jun phosphorylation when PC12 cells are treated with Fe_3O_4-NPs (Fig. 8D). After 24 h of treatment with Fe_3O_4-NPs, PC12 cells also show an increase in the phosphorylation levels of p53, a protein that is involved in the G2/M DNA damage checkpoint and promotes apoptosis (Fig. 8E). And densitometry analysis for Western blot had been showed in Table 1.It was confirmed that Fe_3O_4-NPs induce the dose-dependent expression of p21, Gadd45, bax, and bcl-2; these proteins are all downstream of p53 in regulating the cell cycle and apoptosis (Fig. 8E).

4. Discussion and conclusions

It has become increasingly evident that environmental factors contribute to the development of neurodegenerative diseases, such as Parkinson's disease and Alzheimer's disease (Calderon-Garciduenas et al., 2004). Peters et al. stressed the importance of characterising nanoparticle-related oxidative stress in the brain. It is also important to evaluate the connection between neurodegenerative diseases and long-term nanoparticle exposure (Peters et al., 2006). As Fe_3O_4-NPs applications continue to be found in the life science and industrial fields, the risk of occupational nanoparticle exposure rises correspondingly. It was reported that the inhalation of ultrafine particulate material in polluted air contributes to protein fibrillation; the enhancement of Aβ42 and α-synuclein fibrillation may play a role in the development of Alzheimer's and Parkinson's diseases (Calderón-Garcidueñas et al., 2008). However, little is known about the potential adverse effects of Fe_3O_4-NPs on brain function and whether respiratory exposure is correlated with the onset of neurodegenerative disorders.

Our laboratory has previously used ^{125}I-SiO_2-NPs to investigate the distribution of nanoparticles in tissue; our results indicated that this isotopic tracer technique was appropriate for the quantisation of nanoparticles *in vivo* (Xie et al., 2010). Marquis reports that the distribution and metabolism of nanoparticles will be affected when labelling nanoparticle isotopes *in vivo* (Marquis et al., 2009). Our studies have shown that ^{125}I labelled Fe_3O_4-NPs are spherical, negatively charged, and approximately the same size as unlabelled nanoparticles (Fig. 2). Instant thin layer chromatography-silica gel (ITLC-SG) and stability analysis indicate that radioactive iodine-labelled nanoparticles have a high purity and good stability (Fig. 3). As a result, we were confident that the biological behaviour of ^{125}I-Fe_3O_4-NPs *in vivo* would not differ significantly from that of unlabelled nanoparticles in our subsequent studies.

The striatum is responsible for regulating autokinetic stability, muscular tension, and posture; neuronal damage to the striatum is closely correlated with Parkinson's disease. Injury to the hippocampus may also initiate dysmnesia and the eventual onset of senile dementia. Our findings are noteworthy in that the striatum, hippocampus, and olfactory bulb appear to be the major sites of intranasally instilled Fe_3O_4-NP accumulation (Fig. 4A) (Miller et al., 2006). Seven days following the continuous intranasal instillation of Fe_3O_4-NPs for instance, approximately 80% of the nanoparticles remained in the striatum. More than half of the Fe_3O_4-NPs deposited in the striatum and hippocampus remained in these regions 14 days post instillation. Although there has been extensive literature reviewing the translocation of nanoparticles into the brain through the olfactory nerve, the details of Fe_3O_4-NP clearance from brain tissue remain unknown (Wang et al., 2008a,b,c; Elder et al., 2006). A wealth of epidemiological and experimental studies has outlined the long-term effects of the deposition of nanoparticles in liver and lung tissues; the deposition of nanoparticles appears to induce liver cell necrosis (Xie et al., 2010) or inflammatory responses in the lung (Donaldson et al., 2006). The high surface activity of nanoparticles deposited for the long term in the brain may contribute to cellular interaction and free radical production; these reactions cause brain damage and increase the risk of developing neurodegenerative disorders (Sun et al., 2011). Therefore, it is necessary to study the potential of Fe_3O_4-NPs to cause oxidative injuries in the brain.

Brain tissue is more vulnerable than many other tissue types to oxidative stress due to its high metabolic rate, low levels of endogenous scavengers, and extensive networks of axons and dendrites (Cui et al., 2004). In many neurodegenerative disorders, irreversible neuronal death in the brain has been shown to be a response to excessively accumulated ROS. H_2O_2 has traditionally been regarded as a by-product of ROS and implicated in transcription factor activation (Tabata et al., 2012). H_2O_2 may also have a role in instigating neurodegenerative disease. GSH-PX and SOD are key antioxidant enzymes in the body that play crucial roles in maintaining the stability of cellular redox (Hodková et al., 2010). MDA is a marker of oxidative degradation of cell membrane lipids; this process is also known as lipid peroxidation (Demirbilek et al., 2011). For the instillation groups shown in Fig. 5, the striatum exhibited a greater vulnerability to oxidative stress. Stress levels were indicated by elevated H_2O_2 levels and significantly decreased GSH-PX activity compared with the control on the seventh day ($p < 0.05$). Oxidative damage was still obvious in the striatum seven days following nanoparticle instillation (Fig. 5A). These data indicate that the adverse biological effects of nanoparticle exposure persist after nanoparticle clearance, which enhances the risk of nanoparticle-related neurotoxicity. Prolonged and serious oxidative stress may contribute to the activation of inflammation-related genes and transcription factors such as NF-kB and AP-1 (Nguyen et al., 2007); oxidative stress may also play a role in the onset of neurodegenerative diseases. Thus, the accumulation and retention of Fe_3O_4-NPs in the striatum should be carefully monitored. Apart from H_2O_2, no significant changes in the remaining markers of oxidative stress were observed in the hippocampus (Fig. 5); these results may be due to the lower accumulation and retention levels of Fe_3O_4-NPs in the hippocampus. Notably, no pathological changes were observed in the brains exposed to nanoparticles compared with the physiological saline-exposed controls. We speculate that the slight increase in oxidative stress biomarkers does not affect cellular integrity or tissue morphology in the brain.

PC12 cells were selected to demonstrate the mechanism of striatum injuries *in vitro*. PC12 is a cell line derived from rat adrenal medulla pheochromocytoma. PC12 cells induced to differentiate by NGF have typical dopaminergic neuron characteristics in form and function; differentiated PC12 cells are also a widely used paradigm for neurobiological studies (Ishima et al., 2008). MTT assays and LDH measurements revealed that Fe_3O_4-NP exposure results in a dose-dependent cytotoxicity in PC12 cells; this cytotoxicity is reflected in the mitochondrial enzyme expression and cell membrane damage (Fig. 7A and B). Fe_3O_4-NP-induced cellular oxidative stress is also indicated by elevated ROS levels and lipid peroxidation as well as reduced GSH-PX and SOD levels (Fig. 7C–F). PC12 cell cytotoxicity therefore appears to be caused by oxidative stress, which is a well-documented mechanism for cell

damage induced by nanoparticles. These findings are also corroborated by the results of our *in vivo* experiments.

Fe_3O_4-NPs also exert cytotoxic effects by influencing the cell cycle and apoptosis. For example, cells became arrested at the G2/M phase after 24 h of nanoparticle exposure (Fig. 8A). Arresting at the G2/M phase provides time for these cells to instigate DNA repair and delay cell death. However, cells with impaired DNA repair processes enter apoptosis, as illustrated in Fig. 8B and C.

To explore the molecular mechanisms by which Fe_3O_4-NPs mediate apoptosis and the cell cycle, we measured apoptosis and G2/M checkpoint regulator levels. JNK is a molecule that is activated by oxidative stress; by regulating its downstream transcription factor c-Jun, JNK could modify the activity of numerous proteins. JNK may also modulate several important cellular functions involved in apoptosis, neurodegeneration, cell cycle control and proliferation (Coffey et al., 2002). P53 is involved in apoptotic redox mechanisms (Polyak et al., 1997), induces the pro-apoptotic bax protein, and suppresses the apoptosis inhibitor bcl-2 (Miyashita et al., 1994). In the present study, we observed that Fe_3O_4-NP treatment of PC12 cells instigated JNK and c-Jun phosphorylation (Fig. 8D). Moreover, the results demonstrate that the phosphorylation of p53 at ser15 occurs in response to cellular Fe_3O_4-NP exposure and is associated with increased levels of bax and decreased levels of bcl-2. Previous reports have also demonstrated that exposure to nanosilver (Hsin et al., 2008) or silica nanoparticles induces (Liu and Sun, 2010) JNK and p53 activation, upregulation of bax and inhibition of bcl-2; nanoparticle exposure thus results in apoptosis in NIH3T3 and human umbilical vein endothelial cells. The activation of the cell cycle checkpoint protein p53 may delay G2/M to allow DNA repair before replication or mitosis; the delay in G2/M may occur through an increased expression of the p53 downstream effectors p21 and Gadd45 (Han et al., 2003). Western blot analysis revealed that Fe_3O_4-NP exposure led to an increase in p21 and Gadd45 expression; this change implies that Fe_3O_4-NPs mediate a signalling pathway for G2/M arrest. It had been reported found that titanium dioxide nanoparticles activate p53-mediated DNA damage checkpoint signals (Kong et al., 2008). These preliminary findings illustrate several possible molecular mechanisms behind Fe_3O_4-NP-induced apoptosis and G2/M delay in PC12 cells.

In summary, this study indicates that Fe_3O_4-NPs are deposited and retained in the striatum after intranasal instillation; the nanoparticles may then cause oxidative damage in the striatum. The results of our *in vitro* studies on dopaminergic neurons demonstrate that Fe_3O_4-NP exposure decreases cell viability and induces remarkable oxidative stress. Furthermore, we propose the following Fe_3O_4-NP-mediated apoptosis signalling pathway: JNK and c-Jun phosphorylation, p53 phosphorylation, Bax upregulation, Bcl-2 downregulation, apoptosis. We also propose the following Fe_3O_4-NP-mediated pathway for G2/M arrest: JNK, c-Jun and p53 phosphorylation, p21 and Gadd45 upregulation, G2/M arrest. Our study results suggest that it is critical to further investigate how environmental exposure to Fe_3O_4-NPs may contribute to neurotoxicity and the development of neurodegenerative diseases.

Conflict of interest statement

There is no conflict of interest to declare.

Acknowledgments

This work was supported by grants from the Natural Science Foundation of China (nos. 81271700, 30870680), and the Shanghai Sci-Tech Committee Foundation (no. 11DZ2291700), and National Key Technology R&D Program (2012BAI22B01).

References

Appenzeller LM, Munley SM, Hoban D. Subchronic feeding study of herbicide-tolerant soybean DP-35643-5 in Sprague-Dawley rats. Food Chem Toxicol 2008;46:2201–13.

Calderon-Garciduenas L, Reed W, Maronpot RR, Henriquez-Roldan C, Delgado-Chavez R, Calderon-Garciduenas A, et al. Brain inflammation and Alzheimer's-like pathology in individuals exposed to severe air pollution. Toxicol Pathol 2004;32:650–8.

Calderón-Garcidueñas L, Solt AC, Henríquez-Roldán C. Long-term air pollution exposure is associated with neuroinflammation, an altered innate immune response, disruption of the blood-brain barrier, ultrafine particulate deposition, and accumulation of amyloid beta-42 and alpha-synuclein in children and young adults. Toxicol Pathol 2008;36:289–310.

Cui K, Luo X, Xu K, Ven Murthy MR. Role of oxidative stress in neurodegeneration: recent developments in assay methods for oxidative stress and nutraceutical antioxidants. Prog Neuropsychopharmacol Biol Psychiatry 2004;28:771–99.

Coffey ET, Smiciene G, Hongisto V, Cao J, Brecht S, Herdegen T, et al. c-Jun N-terminal protein kinase (JNK) 2/3 is specifically activated by stress, mediating c-Jun activation, in the presence of constitutive JNK1 activity in cerebellar neurons. J Neurosci 2002;22:4335–45.

Demirbilek ME, Demirbilek M, Karahaliloğlu Z. Oxidative stress parameters of L929 cells cultured on plasma-modified PDLLA scaffolds. Appl Biochem Biotechnol 2011;164:780–92.

Donaldson K, Aitken R, Tran L, Stone V, Duffin R, Forrest G, et al. Carbon nanotubes: a review of their properties in relation to pulmonary toxicology and workplace safety. Toxicol Sci 2006;92:5–22.

Elder A, Gelein R, Silva V, Feikert T, Opanashuk L, Carter J, et al. Translocation of inhaled ultrafine manganese oxide particles to the central nervous system. Environ Health Perspect 2006;114:1172–8.

Han C, Demetris AJ, Michalopoulos GK, Zhan QM, Shelhamer JH, Wu T. PPAR gamma ligands inhibit cholangiocarcinoma cell growth through p53-dependent GADD45 and p21(WAF1/Cip1) pathway. Hepatology 2003;38:167–77.

Hood E. Nanotechnology: looking as we leap. Environ Health Perspect 2004;112:A740–9.

Hsin YH, Chena CF, Huang S, Shih TS, Lai PS, Chueh PJ. The apoptotic effect of nanosilver is mediated by a ROS- and JNK-dependent mechanism involving the mitochondrial pathway in NIH3T3 cells. Toxicol Lett 2008;179:130–9.

Hodková A, Cerná P, Kotyzová D, Eybl V. The effect of iron (III) on the activity of selenoenzymes and oxidative damage in the liver of rats. Interaction with natural antioxidants and deferiprone. Hemoglobin 2010;34:278–83.

Ishima T, Nishimura T, Iyo M, Hashimoto K. Potentiation of nerve growth factor-induced neurite outgrowth in PC12 cells by donepezil: role of sigma-1 receptors and IP3 receptors Progr NeuroPsychopharm Biol Psychiatry 2008;32:1656–9.

Kong SJ, Kim BM, Lee YJ, Chung HW. Titanium dioxide nanoparticles trigger p53-mediated damage response in peripheral blood lymphocytes. Environ Mol Mutagen 2008;49:399–405.

Liao CM, Chiang YH, Chio CP. Assessing the airborne titanium dioxide nanoparticle-related exposure hazard at workplace. J Hazard Mater 2009;162:57–65.

Liu X, Sun J. Endothelial cells dysfunction induced by silica nanoparticles through oxidative stress via JNK/P53 and NF-kappaB pathways. Biomaterials 2010;31:8198–209.

Marquis BJ, Love SA, Braun KL. Analytical methods to assess nanoparticle toxicity. Analyst 2009;134:425–39.

Maynard AD, Kuempel ED. Airborne nanostructured particles and occupational health. J Nanopart Res 2005;7:587–614.

Miyashita T, Krajewski S, Krajewska M, Wang HG, Lin HK, Liebermann DA, et al. Tumor-suppressor p53 is a regulator of bcl-2 and bax gene-expression in vitro and in vivo. Oncogene 1994;9:1799–805.

Miller RM, Kiser GL, Kaysser-Kranich TM, Lockner RJ, Palaniappan C, Federoff HJ. Robust dysregulation of gene expression in substantia nigra and striatum in Parkinson's disease. Neurobiol Dis 2006;21:305–13.

Nguyen HX, O'Barr TJ, Anderson AJ. Polymorphonuclear leukocytes promote neurotoxicity through release of matrix metalloproteinases, reactive oxygen species, and TNF-alpha. J Neurochem 2007;102:900–12.

Oszlánczi G, Papp A, Szabó A. Nervous system effects in rats on subacute exposure by lead-containingnanoparticles via the airways. Inhal Toxicol 2011;23:173–81.

Peters A, Veronesi B, Calderón-Garcidueñas L. Translocation and potential neurological effects of fine and ultrafine particles a critical update. Part Fibre Toxicol 2006;3:13–9.

Pisanic TR, Blackwell JD, Shubayev VI, Finones RR, Jin S. Nanotoxicity of iron oxide nanoparticle internalization in growing neurons. Biomaterials 2007;28:2572–81.

Polyak K, Xia Y, Zweier JL, Kinzler KW, Vogelstein B. A model for p53-induced apoptosis. Nature 1997;389:300–5.

Sun L, Li Y, Liu X. Cytotoxicity and mitochondrial damage caused by silica nanoparticles. Toxicol In Vitro 2011;25:1619–29.

Tabata S, Ikeda R, Yamamoto M. Thymidine phosphorylase enhances reactive oxygen species generation and interleukin-8 expression in human cancer cells. Oncol Rep 2012;28:895–902.

Takenaka S, Karg E, Roth C, Schulz H, Ziesenis A, Heinzmann U, et al. Pulmonary and systemic distribution of inhaled ultrafine silver particles in rats. Environ Health Perspect 2001;109:547–51.

Tin Tin Win S, Yamamoto S, Ahmed S, Kakeyama M, Kobayashi T, Fujimaki H. Brain cytokine and chemokine mRNA expression in mice induced by intranasal instillation with ultrafine carbon black Toxicol Lett 2006;163:153–60.

Wang JX, Chen CY, Liu Y, Jiao F, Li W, Lao F, et al. Potential neurological lesion after nasal instillation of TiO2 nanoparticles in the anatase and rutile crystal phases. Toxicol Lett 2008;183:72–80.

Wang JX, Liu Y, Jiao F, Lao F, Li W, Gu YQ, et al. Time-dependent translocation and potential impairment on central nervous system by intranasally instilled TiO2 nanoparticles. Toxicology 2008;254:82–90.

Wang B, Feng WY, Zhu MT, Wang Y, Wang M, Gu YQ, et al. Neurotoxicity of low-dose repeatedly intranasal instillation of nano- and submicron-sized ferric oxide particles in mice. J Nanopart Res 2009;11:41–53.

Wang J, Liu Y, Jiao F. Time-dependent translocation and potential impairment on central nervous system by intranasally instilled TiO2 nanoparticles. Toxicology 2008;254:82–90.

Xie G, Sun J, Zhong G, Shi L, Zhang D. Biodistribution and toxicity of intravenously administered silica nanoparticles in mice. Arch Toxicol 2010;84:10.

Yamauchi K, Toida T, Nishimura S. 13-Week oral repeated administration toxicity study of bovine lactoferrin in rats. Food Chem Toxicol 2000;38:503–12.